Chinese Chemical Letters 33 (2022) 1081–1086

Contents lists available at ScienceDirect

Chinese Chemical Letters

journal homepage: www.elsevier.com/locate/cclet

CoCo-PBA/tetrabutylammonium bromide as highly efficient catalyst for CO_2 and epoxides coupling reaction under mild conditions

Munir Ullah Khan[a], Safir Ullah Khan[b], Jiraya Kiriratnikom[a], Shah Zareen[c], Xinghong Zhang[a,*]

[a] MOE Key Laboratory of Macromolecular Synthesis and Functionalization, Department of Polymer Science and Engineering, Zhejiang University, Hangzhou 310027, China
[b] Hefei National Laboratory for Physical Science at the Microscale, School of Life Sciences, University of Science and Technology of China, Hefei 230027, China
[c] National Synchrotron Radiation Laboratory, Department of Chemical Physics and Key Laboratory of Surface and Interface Chemistry and Energy Catalysis of Anhui Higher Education Institutes, University of Science and Technology of China, Hefei 230029, China

ARTICLE INFO

Article history:
Received 19 April 2021
Revised 24 May 2021
Accepted 1 June 2021
Available online 12 June 2021

Keywords:
CO_2 conversion
Cyclic carbonates
Prussian blue analogue
Heterogeneous catalysis
$Co_3[Co(CN)_6]_2$

ABSTRACT

The development of effective and low-energy-consumption catalysts for CO_2 conversion into high-value-added products by constructing versatile active sites on the surface of heterogeneous compounds is an urgent and challenging task. In this study, a stable and well-defined heterogeneous cobalt hexacyanocobaltate ($Co_3[Co(CN)_6]_2$), typical cobalt Prussian blue analogue (CoCo-PBA) modified with tetrabutylammonium bromide (TBAB), is proven to be the superior catalyst for CO_2 and epoxide coupling to produce cyclic carbonates with > 99% yield under mild reaction conditions (1.0 MPa, 65 °C). Based on a series of characterizations, it is revealed that the CoCo-PBA structure can maintain relatively high thermal and chemical stability. Recycling experiments exhibited that the CoCo-PBA system could retain 98% of the original activity after six reaction rounds. The CoCo-PBA/TBAB catalytic system was also highly active for coupling CO_2 with other industrial-grade epoxides. These results show the CoCo-PBA catalytic system potential flexibility and the generality of the catalyst preparation strategy.

Global warming, environmental pollution, ocean acidification caused by greenhouse gasses (mainly carbon dioxide, CO_2) are genuine concerns and threats to humankind [1]. It is vital to develop sustainable CO_2 capture and sequestration (CCS) technologies to limit greenhouse gas emissions [2]. For CO_2 CCS from industrial streams, various strategies and materials, such as amine-based wet scrubbing and solid porous adsorbents, have been developed. The high energy costs, degradation and inefficiency are disadvantages for amine-based wet-scrubbing systems currently used in industry, have led to discovering alternative CCS approaches [3,4]. Meanwhile, as an abundant C1 resource, CO_2 can be turned into various value-added chemicals and products [5–13]. There is a growing interest in using CO_2 as a raw material resource rather than waste with production costs. From a green and sustainable chemistry perspective, capturing, fixing and transforming CO_2 to cyclic carbonate and other value-added chemicals are fascinating means of effective sequestration; to boost catalytic and industrial growth and reduce global environmental changes triggered by rising CO_2 concentrations [14–18].

Due to their wide range of applications in the pharmaceutical and fine chemical industries, cyclic carbonates produced by CO_2 and epoxide coupling have been of great interest. To date, diverse forms of homogeneous catalysts, including ionic liquids, Schiff bases, metal complexes, *etc.*, have been reported for this reaction; they suffer from an inherent challenge in separating products and recycling catalysts [19–22]. Therefore, it is highly desirable to design heterogeneous catalysts with remarkably high active sites for synthesizing cyclic carbonates, particularly under mild conditions. Conventional solid heterogeneous catalysts, such as metal-organic frameworks (MOFs), zeolites, mesoporous oxides, porous polymers, typically require relatively high temperatures and pressure to activate this reaction due to the CO_2 inert nature [23–26].

Prussian blue analogues (PBAs) and Prussian blue (PB), a diverse family of metal-organic frameworks (MOFs) with a basic cubic lattice crystalline structure, have the general chemical formula $M[M'(CN)_6]$ where M/M′ = transition-metal ions like Co, Fe, Mn, *etc.*). Occupy alternate lattice vertices coordinated octahedrally by bridging cyanide ions (C≡N–) at the lattice edges [27]. Prussian

* Corresponding author.
E-mail address: xhzhang@zju.edu.cn (X. Zhang).

https://doi.org/10.1016/j.cclet.2021.06.002
1001-8417/

blue analogues (PBA) have attained great attention due to their potential applications in CO_2 adsorption, hydrogen gas storage, energy storage, water splitting and low-temperature catalytic reduction of NO_x with NH_3 [28–33]. Several existing zinc-containing water-tolerant ZnCo-PBA and ZnNi-PBA have been evaluated as efficient heterogeneous catalysts for chemical conversion of CO_2 to cyclic carbonates and polycarbonates; high temperature and high-pressure reaction conditions are essential to boost productivity [34,35].

$Co_3[Co(CN)_6]_2$, also known as cobalt(II) hexacyanocobaltate(III), is a mixed-valence homopolynuclear composite with metallic centers connected by cyanide bridges that can be hydrated or anhydrous [36,37]. Dehydration has little impact on its composition, and the only noticeable transition of color is from pink $Co_3[Co(CN)_6]_2{\cdot}nH_2O$ to blue $Co_3[Co(CN)_6]_2$ [38,39]. Zhang and colleagues studied the $Co_3[Co(CN)_6]_2{\cdot}nH_2O$ fine-tuning thermochromic properties; a shift in the coordination environment of Co^{2+} ions with citrate resulted in a color transition from pink to blue upon heating [40]. A similar effect has been observed for PBA-containing films due to changes in the coordination environment of Co^{2+} ions [41].

The immobilization of homogeneous catalysts on heterogeneous catalyst surfaces is a well-known and extensively used procedure [42,43]; however, this technique generally requires cumbersome catalyst preparation procedures. On the other hand, solid catalyst preparation by incorporating organic modifiers is an excellent approach because it is flexible and straightforward. Organic modifiers of amines are typically used for supported noble metal catalysts [44]. Simultaneously, Pd catalysts modified with quinoline derivatives are conventionally employed as Lindlar or Rosenmund catalysts [45]. Noble metal catalysts modified with thiol-based organic modifiers have been utilized for forming self-assembled monolayers [46,47]. Dendrimers, polymers and functional organic acids have also been identified as advantageous modifiers [48–51].

To the best of our knowledge, modification of heterogeneous $Co_3[Co(CN)_6]_2$ catalysts using an ammonium salt has not been reported to date. Therefore, designing a Co^{2+} active site on a PBA surface by modifying it with organic modifiers could provide PBA with new catalytic functions even if the individual active sites are ineffective. In this work, we report that the catalyst composed of $Co_3[Co(CN)_6]_2$ and ammonium salts as the co-catalyst exhibits dramatic activity enhancement for CO_2 and epoxides coupling reaction compared with only $Co_3[Co(CN)_6]_2$ or ammonium salts.

The typical crystal structure of $Co_3[Co(CN)_6]_2$ is illustrated in Fig. 1a, Co^{2+} is bridged by octahedral $[Co(CN)_6]_3^-$ complexes to form a face-centered cubic (fcc) structure with the remaining Co^{2+} locating in the large cavities to balance the charge. In the present study, $Co_3[Co(CN)_6]_2$ was synthesized by a conventional precipitation method. The synthesis and characterization details for $Co_3[Co(CN)_6]_2$ are provided in the Supporting information. Here we synthesized two different Prussian Blue Analogue (PBA); $Co_3[Co(CN)_6]_2$ (abbreviated as CoCo-PBA) and $Fe_3[Co(CN)_6]_2$ (abbreviated as FeCo-PBA). XRD pattern of CoCo-PBA shown in Fig. 1b illustrate intense diffraction peaks showing its good crystallinity and purity.

All the characteristic peaks are in good agreement with reference $Co_3[Co(CN)_6]_2$ phase (JCPDS card No. 04–012–6179). Estimating the average particle size of the $Co_3[Co(CN)_6]_2$ from the XRD data *via* Scherrer equation yields *ca.* 36 nm. The diffractogram for the $Co_3[Co(CN)_6]_2$ showed sharp diffraction peaks at 17.4° (200), 24.7° (220), 35.2° (400), 39.5° (420) and 50° (440) can be assigned to fcc phase crystallographic planes. Figs. 1c and d show transmission electron microscopy (TEM) images of the as-synthesized CoCo-PBA, revealing the formation of a nanoflakes-like structure. The TEM images indicate CoCo-PBA nanoflakes diameters, which vary within 30–50 nm. SEM-EDX data obtained from the CoCo-PBA presented in Fig. S1 (Supporting information) verifies the presence of C, N, O and Co. CoCo-PBA was composed of 28 wt% C, 24 wt% N, 17 wt% O and 31 wt% Co with atomic composition $C_{0.41}N_{0.30}O_{0.19}Co_{0.10}$. For comparison, we also prepared FeCo-PBA nanocubes under the same reaction procedure. The representative TEM images of FeCo-PBA in Fig. S2 (Supporting information) reveals a well-defined cube shape with sizes in the range of 100–300 nm.

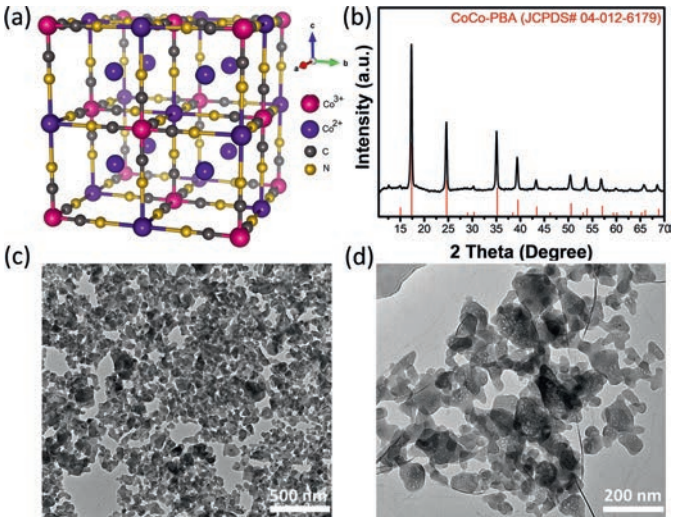

Fig. 1. (a) Crystal structure of $Co_3[Co(CN)_6]_2$. (b) Wide-angle XRD patterns of CoCo-PBA. (c, d) TEM images of CoCo-PBA nanoflakes.

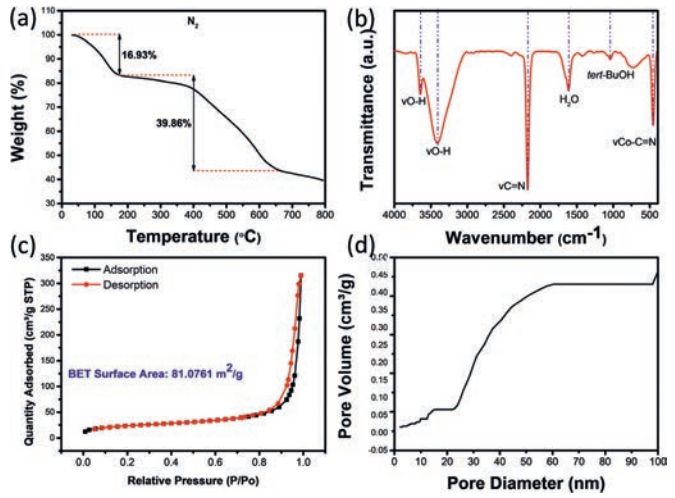

Fig. 2. (a) TGA curve of CoCo-PBA under N_2 atmosphere with a ramp of 10 °C/min. (b) FTIR spectra of CoCo-PBA in KBr pellets. (c) N_2 adsorption/desorption isotherm curve of CoCo-PBA. (d) Pore volume distribution of the pore size.

Thermogravimetric analysis (TGA) under flowing N_2, shown in Fig. 2a, was applied to determine the as-prepared sample thermal decomposition behavior. Two decomposition steps are apparent in the TGA curve. The first step exhibits a weight loss of 16.93% at about 180 °C, illustrating *tert*–BuOH and adsorbed lattice water evaporation. The second step reveals a shift in the TGA curve with a weight loss of 39.86% near the temperature of 650 °C resulting from the sample thermal decomposition.

Fourier transform infrared spectroscopy (FTIR) data in Fig. 2b, shows that the broad IR feature at 3410 cm^{-1} can be readily assigned to the stretching mode of H_2O (ν(O–H)), which is typical of uncoordinated water. More importantly, $Co_3[Co(CN)_6]_2$ characteristic peak at 3644 cm^{-1} can be associated with the cobalt hy-

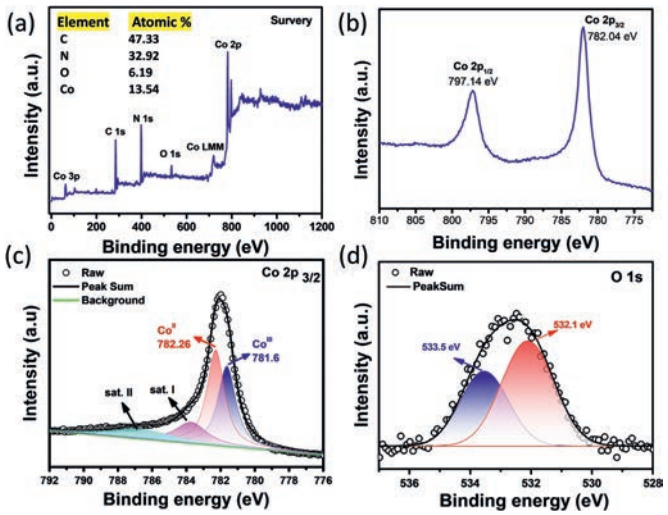

Fig. 3. (a) X-ray photoelectron spectroscopy (XPS) survey spectra of CoCo-PBA. (b, c) High-resolution Co 2p XPS spectrum of CoCo-PBA. (d) High-resolution O 1s XPS spectrum of CoCo-PBA.

droxyl (Co–OH) bond, attributed to the stretching mode of water molecules bound to the metallic centers [52,53], which could dominate the catalytic performances in CO_2 and epoxide coupling reaction.

Excess cobalt ions in the crystal must be counterbalanced by more negatively charged ions to meet the electric neutrality. Besides Cl^- and CN^-, the exclusive negative ion in the CoCo-PBA catalyst was OH^-, which originated from the precipitation reaction of $K_3Co(CN)_6$ and excess $CoCl_2{\cdot}6H_2O$, which is easy to be hydrolyzed. Herein, Cl^- and OH^- served as negative ions for cobalt ions. Presumably, Cl^- in CoCo-PBA served as a good leaving group (like *tert*–BuOH and H_2O) and provided vacant sites for attacking species. The high-intensity IR band at 2174 cm^{-1} can be ascribed to ν(C≡N) in the Co^{3+}–C≡N–Co^{2+} fragment for CoCo-PBA nanoparticles. The IR signal at 1609 cm^{-1} can be assigned to $\delta(OH_2)$, showing the presence of lattice crystal water [54]. Assignment of the weak signal at 1040 cm^{-1} could be associated with *tert*–BuOH in the CoCo-PBA. Additional medium intensity IR signals were observed at 454 cm^{-1} and attributed to ν(Co–C≡N) of cobalt Prussian blue analogue [28,55]. Overall, the hybrid material spectrum was the superposition of $Co_3[Co(CN)_6]_2$.

The mesoporous structures of the as-synthesized samples were further probed by N_2 adsorption–desorption analysis. Before analysis, the catalyst was dried entirely at 60 °C for 24 h under vacuum. The catalyst mesoporous nature could be confirmed by a typical type IV isotherm (IUPAC classification). The CoCo-PBA BET surface area was 81.07 m^2/g, and FeCo-PBA was 23.99 m^2/g (Figs. 2c and d). The highest surface area for CoCo-PBA is closely related to its mesoporous structure. The average pore size of CoCo-PBA was around 24 nm, as shown in Table S1 (Supporting information), which indicates that CoCo-PBA is mesoporous. The heterogeneous mesoporous system is favorable for the catalysis process. The mesoporous nature of CoCo-PBA accelerates the mass transfer of reactants and products in CO_2 and epoxide coupling reactions.

XPS analysis was carried out to determine the surface chemical states of the elements present in the sample. The XPS full survey scan shown in Fig. 3a was collected in the range of 0–1400 eV and confirmed Co 2p, O 1s, N 1s and C 1s peaks. The CoCo-PBA surface contained a large amount of carbon (47.33 at%) and nitrogen (32.92 at%) primarily due to cyanide species of CoCo-PBA with the contribution of adventitious C species associated with the *tert*–BuOH. The CoCo-PBA surface also revealed 6.19 at% oxygen and 13.54 at% cobalt. Differences between the relative Co elemental composition values obtained by SEM-EDX (Fig. S1) instead of XPS (Fig. 3a) can be explained by considering that SEM-EDX measurements involve a spot size (beam size) that is only a few nanometers in diameter.

On the other hand, more prominent spot size is irradiated by X-rays with a dimeter in the millimeter range during the XPS measurements. However, both the current SEM-EDX and XPS experiments explicitly verify C, N, O and Co presence in the CoCo-PBA. The deconvolution of the XPS high-resolution spectra of Co 2p in $Co_3[Co(CN)_6]_2$ consists of two spin-orbit doublets Co $2p_{1/2}$ and Co $2p_{3/2}$ (Fig. 3b). The difference in the binding energy between Co $2p_{1/2}$ and Co $2p_{3/2}$ was 15.1 eV, consistent with literature-reported values [40,55]. Co $2p_{3/2}$ was further fitted into two components to identify the nature of elements present in the sample. The peaks at binding energy 781.6 eV and 782.23 eV were identified as Co^{3+} and Co^{2+}, respectively (Fig. 3c).

Furthermore, two satellite peaks at 783.78 eV and 786.62 eV were observed, which further confirm the presence of Co^{3+} and Co^{2+}, respectively. The O 1s XPS peaks observed in Fig. 3d at 532.1 and 533.6 eV are assigned to the cobalt hydroxyl (Co–OH) and adsorbed water molecules, respectively [56,57]. These results are well consistent with the FTIR results.

The catalytic properties of as-synthesized CoCo-PBA nanoflakes and FeCo-PBA with Tetrabutylammonium bromide (TBAB) as co-catalyst were tested in CO_2 and epoxide coupling reactions under solvent-free conditions. A blank test was conducted without catalyst and TBAB, but no cyclic carbonates were observed. As shown in Table 1, CO_2 and propylene oxide (PO) coupling reactions were catalyzed under the solvent-free conditions at 65 °C and 1 MPa CO_2 pressure for 7 h in the absence of TBAB or CoCo PBA (entries 2 and 3), the yields were undetectable or significantly low (<17%). However, almost >99% yield of cyclic carbonates was achieved (entry 4) under the same reaction conditions when CoCo-PBA and TBAB were used together in the catalytic system. All of these components are essential for catalytic CO_2 and epoxide coupling. The higher catalytic activity of CoCo-PBA can be attributed to the heterogeneous catalyst synergistic interaction with quaternary ammonium salts. Many other catalytic systems have already proved this phenomenon for the CO_2 and epoxide coupling [58–60]. To demonstrate the necessity of CoCo-PBA in this system for catalysis, a control experiment was conducted with FeCo-PBA. Under similar reaction conditions, the target product yield dramatically drops to 36% with the exchange of $Co^{2+}$with Fe^{2+} in FeCo-PBA (entry 5). The yield enhancement of cyclic carbonates was hardly noticeable on other PBAs, indicating that Co^{2+} cooperative interactions in CoCo-PBA and TBAB as the co-catalyst are essential to achieving a high catalytic activity.

We further examined the performances of CoCo-PBA in CO_2 coupling reactions with different highly functionalized industrial-grade terminal epoxides substrates under mild conditions. As shown in Table 1 (entries 6 and 7), small epoxide substrates with electron-donating/- withdrawing groups can be efficiently transformed by CoCo-PBA into corresponding cyclic carbonates with higher yields. Under the same reaction conditions, 1,2-butylene oxide attained nearly >99% yield of 1,2-butylene carbonate, and electron-withdrawing epichlorohydrin produced >99% of 3-chloropropylene carbonate. Interestingly, cyclic carbonate production significantly decreased with gradually increasing molecular sizes of industrial-grade terminal epoxide substrates. As indicated by the 93% formation of 3–*tert*-butoxy-1,2-propylene carbonate (entry 8), 64% formation of 1-phenyl-1,2-ethylene carbonate (entry 9), and 66% formation of 3-phenoxy-1,2-propylene carbonate (entry 10), from *tert*–butyl glycidyl ether, styrene oxide, and phenyl glycidyl ether, respectively. The lower yields could be possibly attributed to considerable steric hindrance, limiting diffu-

Table 1
CoCo-PBA catalyzed CO_2 and epoxides coupling reaction.

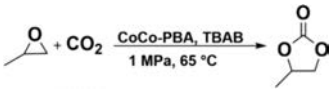

Entry	Catalyst	Epoxide	Product	Yield (%)
1	Blank			0
2	CoCo-PBA			1
3	TBAB			17
4	CoCo-PBA/TBAB			>99
5	FeCo-PBA/TBAB			36
6	CoCo-PBA/TBAB		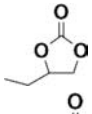	>99
7	CoCo-PBA/TBAB		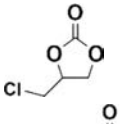	>99
8	CoCo-PBA/TBAB	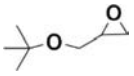	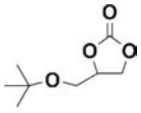	93
9	CoCo-PBA/TBAB	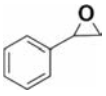	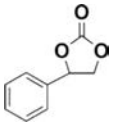	64
10	CoCo-PBA/TBAB	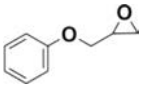	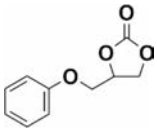	66

Reaction conditions: epoxide (25.0 mmol), TBAB (0.5 mmol), and CoCo-PBA (1 mg) under 1 MPa of CO_2 at 65 °C for 7 h. The yield was determined by ^1H NMR.

sion of the large-sized industrial-grade terminal epoxide substrates into the narrow pores of CoCo-PBA catalyst hence exhibiting size-selective catalysis [61–65].

We tested the performances of CoCo-PBA in CO_2 and epoxide coupling reactions with different alkyl quaternary ammonium salts of bromine. When TBAB was replaced by other alkyl quaternary ammonium salts of bromine, the yield of cyclic carbonates was significantly reduced. Tetramethylammonium bromide attained only a 3.4% yield of cyclic carbonate shown in Fig. S16 (Supporting information), dodecyltrimethylammonium bromide yielded 21% cyclic carbonate (Fig. S17 in Supporting information), and hexadecyltrimethylammonium bromide (CTAB) produced 7.32% cyclic carbonates under the same reaction conditions (Fig. S18 in Supporting information). These results indicated that tetrabutylammonium bromide (TBAB) could interact very well with CoCo-PBA to obtain *a* >99% yield of cyclic carbonates compared to other quaternary ammonium salts of bromine.

Accordingly, the catalytic performance of the CoCo-PBA was worthy of further investigation by determining the cyclic carbonates yield with time. The cyclic carbonates attained almost >99% yield after 7 h (Fig. 4a).

Furthermore, CoCo-PBA catalyst stability was examined by recycling the catalyst. The recycling experiments were carried out over the used CoCo-PBA catalyst recovered from the CO_2 and epoxide coupling reaction by centrifuging, washing, and drying process together with the addition of TBAB for each recycling experiment. After six reaction rounds, about 98% of the original activity was well preserved (Fig. 4b), indicating that the CoCo-PBA catalyst was recyclable without significant activity loss. The high stability of the CoCo-PBA is of vital importance for future applications in industrial processes.

Previous reports for CO_2 and epoxides coupling over various catalysts suggested that surface hydroxyl functional group existence plays a significant role in the ring-opening of epoxides

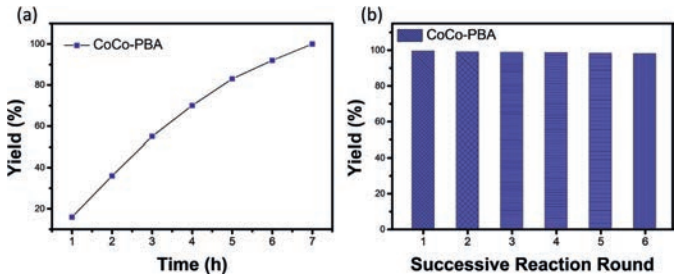

Fig. 4. (a) Time course of the CO_2 and epoxide coupling catalyzed by CoCo-PBA. (b) Product yields achieved with CoCo-PBA over six rounds of successive reactions.

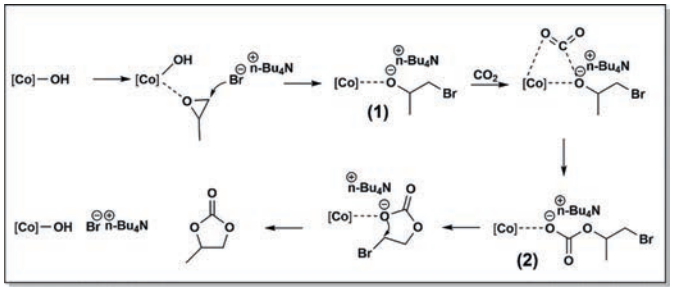

Scheme 1. Proposed mechanism for CO_2 and epoxide coupling catalyzed by the CoCo-PBA.

[34,66,67]. Based on the above experimental results, a possible mechanism of CO_2 and epoxides coupling reaction catalyzed by CoCo-PBA system was proposed (Scheme 1). Co−OH bond on the surface of CoCo-PBA can represent a Lewis acid site (Co^{2+}) associated with a surface hydroxyl (OH^-) Lewis base site. The epoxide was adsorbed and coordinated with the Lewis acid Co site through the epoxide oxygen atom. The nucleophilic attack of the bromide ion from TBAB on the less sterically hindered C atom leads to the activated epoxide ring-opening step, resulting in intermediate **1**. Subsequently, CO_2 was inserted into the cobalt-alkoxide intermediate **1**, producing the anionic intermediate **2**. Finally, intramolecular cyclization results in cyclic carbonate formation, accompanied by the acid site and quaternary ammonium salt regeneration. Furthermore, the excellent performance of the catalyst can be attributed to the proximity between surface hydroxyl (OH^-) functional groups and strong nucleophilic reagents Br^-.

In summary, we have investigated for the first time that heterogeneous catalyst $Co_3[Co(CN)_6]_2$ exhibited superior performance towards CO_2 and epoxides coupling in the presence of TBAB under relatively mild conditions. We genuinely believe that the surface hydroxyls and bromide synergistic interactions significantly contributed to the improvement of CO_2 conversion. More importantly, the catalyst was quickly recovered and showed outstanding performance with excellent stability under successive reaction rounds. Finally, the possible reaction pathway of $Co_3[Co(CN)_6]_2$ toward CO_2 and epoxide coupling was proposed. Considering the facile synthesis and large variety of PBAs, we hope that this research will open a new avenue for developing productive PBAs that contain environmentally benign and abundant transition metals as superior CO_2 conversion catalysts.

Declaration of competing interest

The authors declare that they have no known competing financial interests or personal relationships that could have appeared to influence the work reported in this paper.

Acknowledgement

We gratefully acknowledge the financial support of the National Natural Science Foundation of China (Nos. 21774108 and 51973190).

Supplementary materials

Supplementary material associated with this article can be found, in the online version, at doi:10.1016/j.cclet.2021.06.002.

References

[1] C. Song, Catal. Today 115 (2006) 2–32.
[2] S. Chu, Science 325 (2009) 1599–1599.
[3] N. MacDowell, N. Florin, A. Buchard, et al., Energy Environ. Sci. 3 (2010) 1645–1669.
[4] S. Choi, J.H. Drese, C.W. Jones, Chem. Sustain. Energy Mater. 2 (2009) 796–854.
[5] M.U. Khan, L. Wang, Z. Liu, et al., Angew. Chem. Int. Ed. 55 (2016) 9548–9552.
[6] Q. Yang, C.C. Yang, C.H. Lin, H.L. Jiang, Angew. Chem. Int. Ed. 58 (2019) 3511–3515.
[7] X. Jiang, X. Nie, X. Guo, et al., Chem. Rev. 120 (2020) 7984–8034.
[8] I. Omae, Coord. Chem. Rev. 256 (2012) 1384–1405.
[9] T. Zheng, K. Jiang, H. Wang, Adv. Mater. 30 (2018) 1802066.
[10] K. Li, B. Peng, T. Peng, ACS Catal. 6 (2016) 7485–7527.
[11] M. Ding, R.W. Flaig, H.L. Jiang, O.M. Yaghi, Chem. Soc. Rev. 48 (2019) 2783–2828.
[12] H. Hu, D. Zhang, H. Liu, et al., Chin. Chem. Lett. 32 (2021) 557–560.
[13] P. Jing, B. Wu, Z. Han, et al., Chin. Chem. Lett. 32 (2021) 3505–3508.
[14] T. Jiang, X. Ma, Y. Zhou, et al., Green Chem. 10 (2008) 465–469.
[15] G. Fiorani, A. Perosa, M. Selva, Green Chem. 20 (2018) 288–322.
[16] X.B. Lu, D.J. Darensbourg, Chem. Soc. Rev. 41 (2012) 1462–1484.
[17] T.K. Pal, D. De, P.K. Bharadwaj, Coord. Chem. Rev. 408 (2020) 213173.
[18] J. Liu, C. Chen, K. Zhang, et al., Chin. Chem. Lett. 32 (2021) 649–659.
[19] J. Liu, G. Yang, Y. Liu, et al., Green Chem. 22 (2020) 4509–4515.
[20] B.H. Xu, J.Q. Wang, J. Sun, et al., Green Chem. 17 (2015) 108–122.
[21] C. Maeda, T. Taniguchi, K. Ogawa, et al., Angew. Chem. Int. Ed. 54 (2015) 134–138.
[22] A. Decortes, A.M. Castilla, A.W. Kleij, Angew. Chem. Int. Ed. 49 (2010) 9822–9837.
[23] M.H. Beyzavi, R.C. Klet, S. Tussupbayev, et al., J. Am. Chem. Soc. 136 (2014) 15861–15864.
[24] K. Huang, J.Y. Zhang, F. Liu, et al., ACS Catal. 8 (2018) 9079–9102.
[25] G. Ji, Z. Yang, H. Zhang, et al., Angew. Chem. 128 (2016) 9837–9841.
[26] D. Liu, G. Li, J. Liu, et al., ACS Appl. Mater. Interfaces 10 (2018) 22119–22129.
[27] A. Simonov, T. De Baerdemaeker, H.L.B. Boström, et al., Nature 578 (2020) 256–260.
[28] L. Hu, P. Zhang, Q. Chen, et al., RSC Adv. 1 (2011) 1574–1578.
[29] S.S. Kaye, J.R. Long, J. Am. Chem. Soc. 127 (2005) 6506–6507.
[30] H. Yi, R. Qin, S. Ding, et al., Adv. Funct. Mater. 31 (2021) 2006970.
[31] L. Deng, Z. Yang, L. Tan, et al., Adv. Mater. 30 (2018) 1802510.
[32] P.Y. Tang, L.J. Han, F.S. Hegner, et al., Adv. Energy Mater. 9 (2019) 1901836.
[33] L. Yan, Y. Liu, K. Zha, et al., ACS Appl. Mater. Interfaces 9 (2017) 2581–2593.
[34] R.J. Wei, X.H. Zhang, et al., J. Mol. Catal. A 379 (2013) 38–45.
[35] X.H. Zhang, S. Chen, X.M. Wu, et al., Chin. Chem. Lett. 18 (2007) 887–890.
[36] M. Cao, X. Wu, X. He, C. Hu, Chem. Commun. (2005) 2241–2243.
[37] L. Hu, J. Mei, Q. Chen, et al., Nanoscale 3 (2011) 4270–4274.
[38] D.H.M. Buchold, C. Feldmann, Chem. Mater. 19 (2007) 3376–3380.
[39] D.F. Shriver, D.B. Brown, Inorg. Chem. 8 (1969) 42–46.
[40] H. Zhang, C. Li, D. Chen, et al., Cryst. Eng. Comm. 19 (2017) 2057–2064.
[41] H.Y. Tang, Z. Chu, C.P. Li, et al., Dalton. Trans. 45 (2016) 10249–10255.
[42] M. Tada, Y. Iwasawa, Chem. Commun. (2006) 2833–2844.
[43] E.L. Margelefsky, R.K. Zeidan, M.E. Davis, Chem. Soc. Rev. 37 (2008) 1118–1126.
[44] T. Bürgi, A. Baiker, Acc. Chem. Res. 37 (2004) 909–917.
[45] M. Hudlicky, in: Reductions in Organic Chemistry, Ellis Horwood Chichester, 1984, pp. 46–53.
[46] C.A. Schoenbaum, D.K. Schwartz, J.W. Medlin, Acc. Chem. Res. 47 (2014) 1438–1445.
[47] S.H. Pang, C.A. Schoenbaum, D.K. Schwartz, J.W. Medlin, Nat. Commun. 4 (2013) 1–6.
[48] J. Luo, X. Zhang, C. Zhang, et al., Chin. Chem. Lett. 30 (2019) 2043–2046.
[49] E. Gross, J.H.C. Liu, F.D. Toste, Nat. Chem. 4 (2012) 947–952.
[50] H. Tsunoyama, N. Ichikuni, H. Sakurai, T. Tsukuda, J. Am. Chem. Soc. 131 (2009) 7086–7093.
[51] X.R. Wang, H.M. Cheng, X.W. Gao, et al., Chin. Chem. Lett. 30 (2019) 919–923.
[52] J.T. Kloprogge, R.L. Frost, J. Solid State Chem. 146 (1999) 506–515.
[53] J. Lejeune, J.B. Brubach, P. Roy, A. Bleuzen, Comptes Rendus Chim. 17 (2014) 534–540.
[54] L. Gao, C. Wang, R. Li, et al., Nanoscale 8 (2016) 8355–8362.
[55] C.L.C. Carvalho, A.T.B. Silva, R.A.S. Luz, et al., ACS Appl. Nano Mater. 1 (2018) 4283–4293.
[56] X. Wang, L. Lu, B. Wang, et al., Adv. Funct. Mater. 28 (2018) 1804191.
[57] M. Chen, Y. Wu, Y. Han, et al., ACS Appl. Mater. Inter. 7 (2015) 21852–21859.

[58] W.Y. Gao, Y. Chen, Y. Niu, et al., Angew. Chem. Int. Ed. 53 (2014) 2615–2619.
[59] Q. Yang, C.C. Yang, C.H. Lin, H.L. Jiang, Angew. Chem. Int. Ed. 58 (2019) 3511–3515.
[60] W.Y. Gao, L. Wojtas, S. Ma, Chem. Commun. 50 (2014) 5316–5318.
[61] G. Si, X. Kong, T. He, et al., Chin. Chem. Lett. 32 (2021) 918–922.
[62] A. Corma, H. Garcia, F.X. Xamena, Chem. Rev. 110 (2010) 4606–4655.
[63] C. Zhu, G. Yuan, X. Chen, Z. Yang, Y. Cui, J. Am. Chem. Soc. 134 (2012) 8058–8061.
[64] S. Horike, M. Dinca, K. Tamaki, J.R. Long, J. Am. Chem. Soc. 130 (2008) 5854–5855.
[65] Y. Chen, V. Lykourinou, T. Hoang, et al., Inorg. Chem. 51 (2012) 9156–9158.
[66] Y. Wang, S. Li, Y. Yang, et al., Chem. Commun. 55 (2019) 6942–6945.
[67] A. Samikannu, L.J. Konwar, P. Mäki-Arvela, et al., Appl. Catal. B 241 (2019) 41–51.